AIAA-99-2856

The Ion Propulsion System on NASA's Space Technology 4/Champollion Comet Rendezvous Mission

J. R. Brophy, C. E. Garner, J. E. Polk,
and J. M. Weiss
Jet Propulsion Laboratory
California Institute of Technology
Pasadena, CA

35th AIAA/ASME/SAE/ASEE Joint Propulsion Conference and Exhibit
20–24 June 1999
Los Angeles, California

AIAA-99-2856

The Ion Propulsion System on NASA's Space Technology 4/Champollion Comet Rendezvous Mission

John R. Brophy, Charles E. Garner, James E. Polk, and Jeffery M. Weiss,
Jet Propulsion Laboratory
California Institute of Technology
Pasadena, California

The ST4/Champollion mission is designed to rendezvous with and land on the comet Tempel 1 and return data from the first-ever sampling of a comet surface. Ion propulsion is an enabling technology for this mission. The ion propulsion system on ST4 consists of three ion engines each essentially identical to the single engine that flew on the DS1 spacecraft. The ST4 propulsion system will operate at a maximum input power of 7.5 kW (3.4 times greater than that demonstrated on DS1), will produce a maximum thrust of 276 mN, and will provide a total ΔV of 11.4 km/s. To accomplish this the propulsion system will carry 385 kg of xenon. All three engines will be operated simultaneously for the first 168 days of the mission. The nominal mission requires that each engine be capable of processing 118 kg. If one engine fails after 168 days, the remaining two engines can perform the mission, but must be capable of processing 160 kg of xenon, or twice the original thruster design requirement. Detailed analyses of the thruster wear-out failure modes coupled with experience from long-duration engine tests indicate that the thrusters have a high probability of meeting the 160-kg throughput requirement.

electric propulsion

Introduction

Space Technology 4 (ST4)/Champollion is the fourth mission in NASA's New Millennium program. The first mission in this series was Deep Space 1 (DS1) which was launched in October, 1998 and demonstrated, for the first time, the use of ion propulsion as the primary propulsion system for a deep-space mission. The objectives for ST4/Champollion are to flight validate technologies, systems and procedures necessary for rendezvous, landing and anchoring a science payload on a comet [1]. In addition, this mission seeks to acquire science data on the properties, composition and morphology of a comet while performing the first-ever sampling and analysis of the surface and subsurface. In situ investigation of a cometary nucleus is expected to provide key data for understanding the origin of the solar system. ST4 is scheduled for an April 2003 launch using a Delta II 7925 and will arrive at the comet Tempel 1 approximately three years later.

The heliocentric ΔV required to catch up to and rendezvous with the comet will be provided by a multi-engine **solar electric propulsion (SEP)** system based on the single-ion-engine system used on DS1. The ST4 multi-engine SEP system is a technology applicable to many other deep-space missions of interest including Mercury Orbiter, Neptune Orbiter, Titan Explorer, Saturn Ring Observer, Europa Lander, Comet Sample Return, and Venus Sample Return, as well as to a variety of near-Earth-space missions. Electric power for the SEP system and the spacecraft will be provided by an advanced a 10-kW (beginning-of-life at 1 AU) solar array having a specific mass of approximately 10 kg/kW.

Why Ion Propulsion for ST4?

The use of ion propulsion for comet rendezvous missions is a dream that has long fascinated mission planners and electric propulsion technologists alike. Serious mission and system studies for comet rendezvous missions began in the 1960's (see for example Refs. 2-4) following the successful operation of the first broad-beam, electron-bombardment ion engine in the laboratory at NASA's Lewis Research Center (now the Glenn Research Center) in 1960 [5]. Numerous comet rendezvous mission studies based on

the use of ion propulsion followed in the subsequent three decades. References 6-20 represent only a small fraction of these studies. Ion propulsion is a natural fit for comet rendezvous and comet sample return missions because the highly elliptical, inclined orbit of a typical short-period comet requires a substantial heliocentric ΔV to transfer a spacecraft between the Earth's orbit and the comet's orbit.

As is characteristic of NASA's new approach to deep-space missions, ST4 is being designed to meet its mission objectives while operating under strict funding constraints. The multi-engine ion propulsion system on ST4 enables the use of the Delta II 7925 launch vehicle. Without the use of SEP, a much larger and more expensive launch vehicle would be required and the ST4/Champollion mission would be unaffordable. This is a direct consequence of the heliocentric ΔV required from the propulsion system. The SEP system for ST4 must provide a total ΔV of approximately 11.4 km/s. To provide an equivalent ΔV with a conventional Earth-storable chemical propulsion system would require an enormous increase in propellant mass and a significantly larger launch vehicle.

For example, the International Rosetta Mission being developed by ESA is being designed to rendezvous with the comet 46P/Wirtanen and is scheduled for launch in January 2003 [21]. The Rosetta spacecraft does not use ion propulsion, instead it has an on-board, bi-propellant propulsion system which provides a ΔV capability of 1.44 km/s (nearly a factor of 8 less than the ΔV capability of the ST4 on-board ion propulsion system). Furthermore, the Rosetta propulsion system requires a propellant mass of 1390 kg compared to 385 kg of xenon for ST4. This results in 46% of the Rosetta spacecraft initial wet mass being propellant. In contrast, only 33% of the ST4 initial mass is propellant even though it provides eight times the ΔV of the Rosetta propulsion system.

The lower ΔV capability of the chemical propulsion system on Rosetta requires that the launch vehicle inject the spacecraft to a significantly higher hyperbolic excess velocity (relative to the Earth) than is required for ST4. In addition, the Rosetta Mission requires a time consuming Mars-Earth-Earth gravity assist trajectory to pick up sufficient energy to rendezvous with the comet resulting in a total trip time of approximately nine years. This is three times the trip time required for ST4 which requires no gravity-assist maneuvers.

NSTAR

The ion propulsion system for ST4 is based on the ion propulsion technology developed under the NSTAR (NASA Solar electric propulsion Technology Application Readiness) program. The objective of this on-going program is to overcome the barriers preventing the use of SEP and enable ion propulsion to enter the mainstream of deep-space propulsion options. Specifically, this program is designed to obtain the information needed by a program manager to baseline the use of ion propulsion on a deep-space mission, to validate ion propulsion technology through the flight test on Deep Space 1, and to transfer this ion propulsion technology from government laboratories to industry and user organizations.

By all measures the NSTAR program has been an outstanding success. Aside from an initial hiccup [22], the operation of the NSTAR ion propulsion system on DS1 has been flawless, and it has successfully provided the ΔV required for the July 29, 1999 flyby of asteroid 1992KD. Consequently, it has resulted in ion propulsion now being a credible propulsion option for deep-space missions.

The ion propulsion system on DS1 consists of a single-string system which includes: one ion engine, one power processing unit (PPU), one digital interface and control unit (DCIU), and one xenon feed system (XFS). In addition, the DS1 spacecraft provides a 2-axis gimbal mechanism capable of pointing the ion engine to $\pm$ 5 degrees in each axis. The NSTAR ion propulsion system is described in detail in Refs. 22-25.

The baseline mission for DS1 includes only the flyby of asteroid 1992KD. In successfully providing the ΔV to meet this mission objective the ion propulsion system operated for a total of 1,800 hours and processed 12 kg of xenon. This resulted in a ΔV imparted to the spacecraft of approximately 740 m/s.

The extended mission for DS1 is to fly by the comets Wilson-Harrington (in January 2001) and Borelly (in September 2001). To accomplish this will require the expenditure of an additional 56 kg of propellant resulting in a total ΔV from the ion propulsion system of about 4.5 km/s.

ST4 Ion Propulsion System

The ST4 spacecraft in its flight configuration is shown in Fig. 1. The ion propulsion system includes three NSTAR ion engines, three PPUs, two DCIUs and

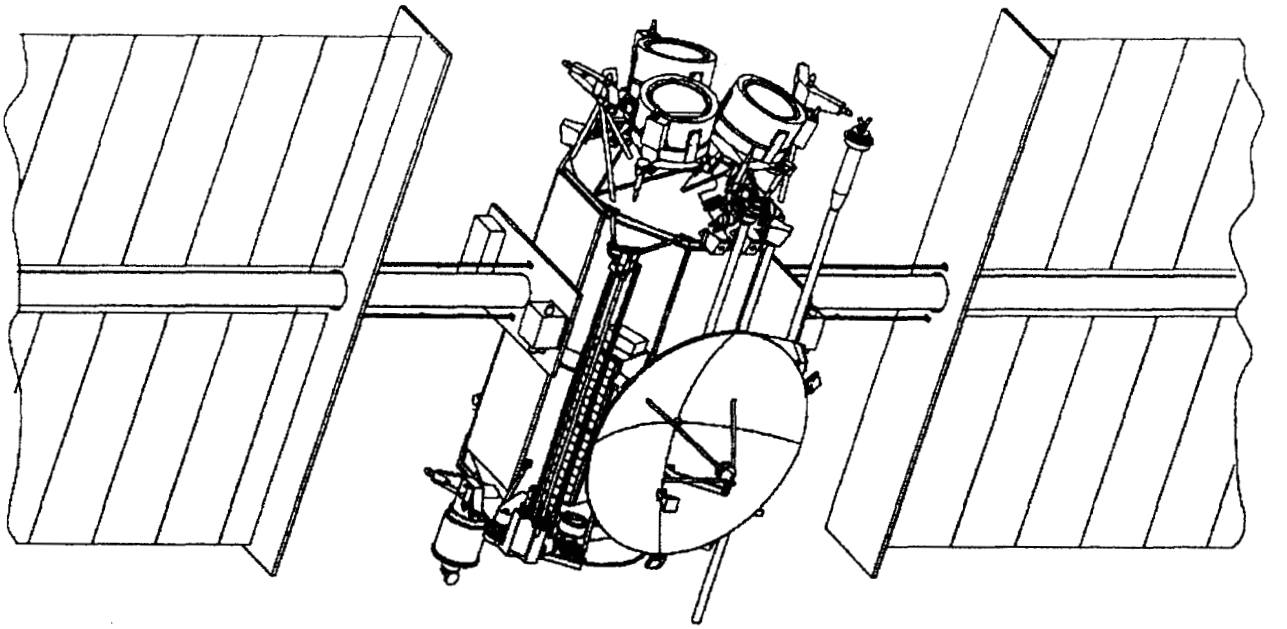

Fig. 1 ST4 spacecraft in the cruise configuration.

an advanced xenon feed system. Each ion engine is attached to a two-axis gimbal mechanism capable of pointing the thruster ± 10 degrees in each axis. The propulsion system is controlled by only one DCIU at a time, the other DCIU is maintained as a cold spare. The PPUs are cross-strapped so that each PPU can operate either of two engines, and each engine is attached to two PPUs. This cross-strapping capability was designed into the NSTAR PPUs in anticipation of this type of configuration.

The advanced xenon feed system replaces the bang-bang pressure regulation system used on DS1 with active pressure regulators based on new components currently under development. Candidates for the pressure regulator include the multifunction valve from Marotta Scientific Controls, Inc. and the proportional solenoid valve from Moog, Inc. The use of these new components enables the elimination of the relatively large and heavy plenum tanks used in the DS1 XFS.

The mass breakdown of the ion propulsion system is given in Table 1. This mass list does not include the masses for the gimbals, the wire harnesses, or the thermal control hardware, all of which are book-kept with other spacecraft subsystems.

Table 1 ST4 IPS Mass List

Component	Qty	Unit Mass (kg)	Total Mass (kg)	Mass Cont. (kg)
Ion Engine	3	8.34	25.02	3.75
PPU	3	14.82	44.46	6.67
DCIU	2	2.80	5.60	1.40
XFS	1	9.34	9.34	2.75
Tank	1	13.80	13.80	3.40
Total			98.22	

The power from the solar array as a function of time into the ST4 mission is given in Fig. 2. The variation in power is due to the changing spacecraft distance from the sun and accounts for the variation in solar cell efficiency with temperature and the effects of radiation damage. The lower curve in this figure is the total power input to the ion propulsion system. The difference between these curves is the power available to the rest of the spacecraft.

The trajectory for ST4 requires that all three of the ion engines operate simultaneously for approximately the first six months of the mission. After the first six months no more than two engines are operated at the

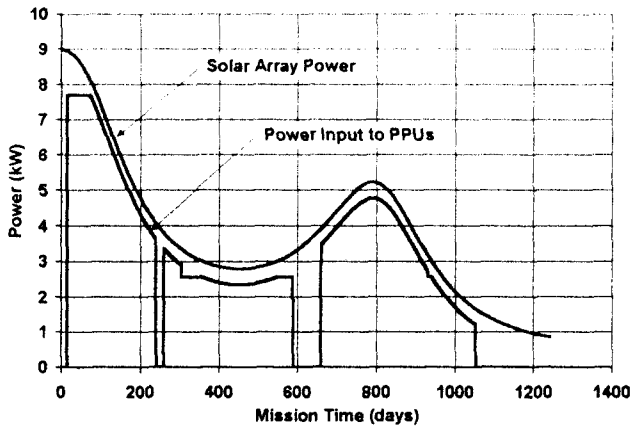

Fig. 2 Solar array power and total PPU input power over the ST4 mission.

same time due to limitations on the available power. The power input to each PPU is given in Fig. 3 as a function of mission time. The lower curve in this figure indicates the number of operating engines. All operating thrusters are assumed to run at the same power level.

An interesting feature of the data in Fig. 3 is that the input power per PPU never falls below about 1.2 kW. This is a consequence of the particular trajectory used for this mission. The NSTAR propulsion hardware can be throttled to a PPU input power as low as 525 W, but this deep-throttling capability is does not appear to be needed for ST4.

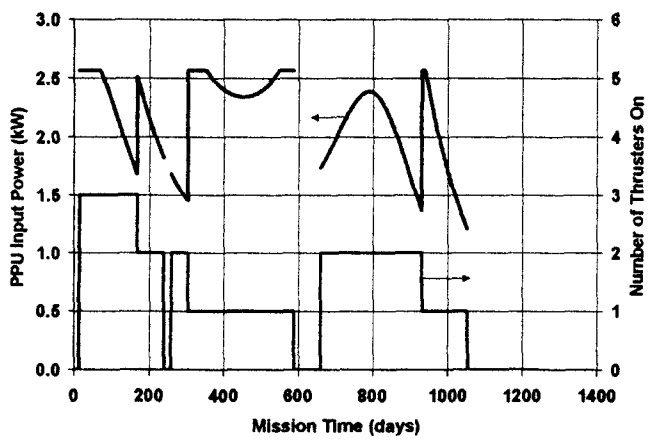

Fig. 3 Input power per PPU.

Multiple Thruster Operation

The ST4 mission requires the simultaneous operation of up to three ion engines. With each engine operating at full power the propulsion system will process approximately 7.5 kW of power and produce a thrust of 276 mN. For this to be successful, undesirable interactions within the ion propulsion system and between the ion propulsion system and the spacecraft must be minimized. Potential interactions may be grouped into five major categories:

1. Thermal – non-uniform heating of adjacent thrusters.
2. Thruster Particle Efflux – effects on coupling voltage, keeper voltages, neutralizer failure, beam plasma potential, and interaction of the primary ion beams.
3. Radiated and Conducted EMI.
4. Effect on Thruster Life -- changes in accelerator grid impingement current, flake containment.
5. DCIU fault management.

A review of the literature indicates several instances where multiple ion engines have been operated simultaneously in the same vacuum test facility [26-32]. In general, this body of experience indicates that operation of multiple ion engines is straight forward.

The thermal environment the thrusters see is strongly dependent on the particulars of the spacecraft configuration. Detailed thermal analyses are required whether or not there are multiple thrusters. The asymmetric heating caused by the operation of adjacent thrusters does, however require a non-axisymmetric thruster thermal model.

There is essentially no interaction of the primary ion beams. The beam current densities downstream of multiple operating thrusters add linearly as if each thruster were operating singly [32]. Operation of multiple thrusters has been observed to have a slight impact the neutralizer coupling voltage and in a way that is not well understood, but the magnitude of the effect is not significant.

Electromagnetic interactions are highly hardware and configuration dependent. Therefore, measurements of these interactions must be made using hardware representative of the flight hardware. There does not, however, appear to be compelling evidence that suggests this hardware must include the thrusters. It appears that sufficient information regarding electromagnetic interactions between PPUs and between the IPS and the spacecraft can be obtained with the PPUs operating into resistive loads.

Two possible mechanisms have been identified to date in which multiple engine operation may impact the engine life. The first of these is the effect on the accelerator grid impingement current. Multiple engine operation will generate more charge-exchange ions than a single engine and it is not known if this will impact the magnitude or distribution of the currents collected by each engine's accelerator grid. If the magnitude increases or the distribution changes, the service life of the accelerator grid could be impacted.

The second mechanism concerns the non-uniform heating of one thruster due to the operation of an adjacent thruster. This non-uniform heating will change the thermal expansion of the thruster possibly impacting the containment of thin sputter-deposited films. Since the behavior of these thin films is not well understood, the degree to which this is a problem cannot be quantified. It should be noted, however, that varying sun angles on a spacecraft with a single ion engine will also result in asymmetric heating of the thruster.

Finally, for multiple engine operation the DCIU must startup, control, and shutdown any combination of the three engines on ST4. The software in the NSTAR DCIU was designed to handle multiple thruster operation, but this feature could not be tested with the single-thruster system on DS1. There appears to be value in testing the DCIU software with multiple PPUs operating multiple real thrusters. Real thrusters, instead of resistive loads, are believed to be necessary to assess potential timing issues and the ability of the DCIU to handle off-nominal conditions.

Engine Throughput Requirement

From the trajectory analyses a total 350 kg of xenon is required to perform this mission. Currently a 10% contingency on the propellant mass is being carried for a total propellant loading of 385 kg. The amount of propellant processed by each engine is given in Fig. 4 vs. mission time. These data indicate that each thruster must process approximately 118 kg of xenon. The NSTAR program has as one of its remaining objectives to demonstrate a total propellant throughput capability per engine of 125 kg. This demonstration is taking place in an on-going Extended Lifetime Test (ELT) at JPL. As of the end of May the thruster had successfully processed approximately 43 kg of xenon. Further details regarding this test are provided by Anderson [33].

The upper curve in Fig. 4 represents the amount of propellant each thruster would have to process if one

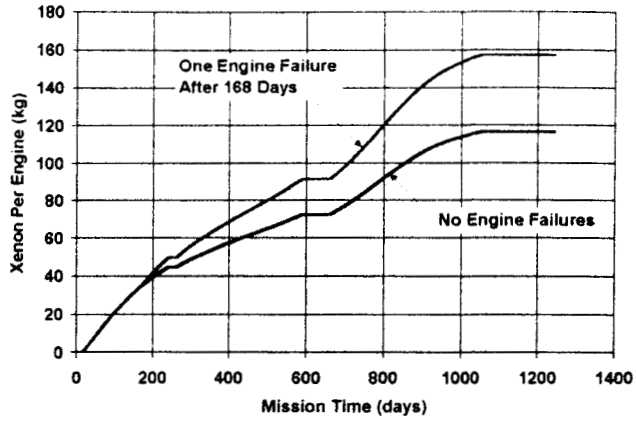

Fig. 4 Throughput required per engine for the ST4 mission.

thruster were to fail six months into the mission (after there is no longer the requirement to operate three thrusters simultaneously). In this case, the remaining thrusters must process a total of nearly 160 kg of xenon each. This is twice the original design goal for the NSTAR thruster. A total throughput of 160 kg is approximately equal to 16,000 hours of operation at full power.

The throughput requirement per thruster could be mitigated by simply adding a fourth thruster to the propulsion system. If this were done the nominal throughput requirement, assuming no thruster failures would be 88 kg per engine. In the case where one thruster fails at the beginning of the mission, the throughput requirement for the remaining thrusters is the same as the current ST4 design with no thruster failures, i.e., 118 kg. The addition of a fourth thruster, however, is not an attractive option because it would result in a significant increase in the mass of the ion propulsion system. This mass increase is the result of the added thruster mass, as well as the mass of another gimbal, additional feed system components, an additional wiring harness, and additional miscellaneous structure. The resulting mass growth of the propulsion system would severely impact the mass budgets the other spacecraft subsystems. Consequently, the ST4 program is strongly motivated to be able to fly with only three ion engines. The critical question is whether the NSTAR ion engines have sufficient throughput capability to perform this mission.

Engine Throughput Capability

NSTAR included as an integral part of the program a task to assess the service life capability of the ion

engine. It was clear at the start of the NSTAR program that if it were to successfully get ion propulsion into the mainstream of propulsion options available for deep-space missions, that there would be an immediate call for improved engine performance. This has indeed happened with ST4 requiring a factor of two increase in the total propellant throughput capability for the engine.

The NSTAR program's service life assessment activity is based on the execution of a few long-duration tests together with probabilistic analyses of the principal damage-accumulation failure modes. This approach was selected based on the demonstrable fact that it is not feasible to establish the failure risk of highly reliable, long-lived systems through testing alone [34]. The progress of this task has been documented in a series of technical papers [34-42].

Prior to the execution of any of the long-duration tests under the NSTAR program probabilistic modeling suggested certain failure modes had relatively high failure probabilities for the desired engine service life [34]. This analysis captured the lack of knowledge associated with the unknown behavior of key driver parameters in the models of the important failure modes and expressed it as an increased risk. As more experience was gained from long-duration tests, the behavior of the key drivers became better understood and this improved knowledge is now reflected as a reduced failure risk at a given service life.

Engine Failure Modes

The role of long-duration testing in establishing the engine service life is to:

1. Identify previously unknown failure modes.
2. Provide information to eliminate analysis oversights or errors.
3. Characterize the parameters which drive the results of the analyses.
4. Characterize the engine performance as a function of time.

Review of the literature of ion engine life testing together with the long-duration tests performed under the NSTAR program have identified the following important potential failure mechanisms for the NSTAR engine.

1. Electron-backstreaming due to enlargement of the accelerator grid apertures by ion sputtering.
2. Structural failure of the accelerator grid due to erosion by ion sputtering.
3. Unclearable short between the screen and accelerator grids due to a flake of material formed from the deposition and subsequent flaking of sputtered material.
4. Depletion of the cathode low-work-function material
5. Unclearable short between the keeper electrode and the cathode due to a flake of material formed from the deposition of material sputtered off the cathode orifice plate.
6. Structural failure of the accelerator grid due to direct ion impingement from defocused beamlets caused by flakes of material on the screen grid.
7. Erosion of the keeper orifice plate resulting in its structural failure.
8. Structural failure of the screen grid due to erosion by ion sputtering.
9. Erosion of the neutralizer orifice plate due to operation in plume mode for extended duration.
10. Cathode heater failure due to thermal cycling.

Each of these failure modes is discussed below in reference to its potential impact to the ST4 mission.

Cathode Heater Failure. Failure due to thermal cycling of the cathode heater is not expected to be a significant risk because at most only a few hundred on/off cycles are required for deep-space missions such as ST4. Extensive testing of the cathode heaters has been performed to verify that they have less than a 1% chance of failure after 6000 cycles [43].

Neutralizer Orifice Plate Failure. Excessive erosion of the neutralizer orifice plate can occur during extended operation in plume mode, a mode characterized by a visible plume coming from the neutralizer. Under normal operating conditions the neutralizer flow rate is set at a level selected to prevent plume-mode operation throughout the engine life. If this selection is done incorrectly it is conceivable that the neutralizer could enter plume mode at some point in the mission due to aging effects. The current neutralizer flow rates have been selected based on data collected in the NSTAR 8,000-hr test [42]. The on-going ELT [33] will provide information regarding the neutralizer behavior beyond 8,000 hours and if necessary the neutralizer flow rate could be increased to assure that the neutralizer stays out of plume mode throughout the mission. This would result in a small overall reduction in the thruster performance.

Screen Grid Structural Failure. Structural failure of the screen grid by ion sputtering has been treated probabilistically [38]. Most of the erosion damage to the screen grid is believed to be caused by multiply charged ions produced in the discharge chamber. Consequently, this failure mode is very sensitive to the ratio of double to single ion production rates, as well as to the potential difference between the screen grid and the discharge chamber plasma. The time to failure of the screen grid is given in [38] as,

$$T_{sg} = \frac{t_s \phi_i f_b e \rho \, A_b (1-\phi_s)\left(1 + f_d R_+^{++}\right)}{J_b m_g (1-\phi_i)\left(Y_+ + \frac{f_d}{2} R_+^{++} Y_{++}\right)} \qquad (1)$$

which simply describes the time required to sputter-erode completely through the screen grid on the centerline of the thruster. All of the symbols in Eq. (1) are defined in Table 2. Also listed in this table are the ranges for each parameter that cannot be specified exactly. The uncertainty in the values of these key parameters is handled probabilistically using a Monte Carlo simulation. A value for each parameter is selected at random from within its allowable range of values. The time to screen grid structural failure, T_{sg}, is then calculated from Eq. (1). The process is repeated typically 100,000 times. Because the values of the input parameters vary, the calculated failure times will form a distribution. This analysis indicates that the peak in the failure distribution shown in Fig. 5 occurs at approximately 27,000 hours of operation at full power. Normalizing this distribution and then integrating over different run times results in the curve of the failure probability versus run time given in Fig. 6. This figure suggests that there is less than 1 chance in 1000 that the screen grid will fail after 16,000 hours of operation at full power, which is equivalent to a throughput of 160 kg.

These calculations assume that all of the xenon is processed at the engine's full power point, an assumption which significantly simplifies the calculations. In reality the engines will be run over the throttling curve given in Fig. 3. It can be shown using Eq. (1), however, that the full power point is the most stressing case. That is, from the standpoint of screen grid failure, the total engine throughput capability is smallest when operated at full power. Therefore, the failure risk curve in Fig. 6 is conservative.

Another major source of uncertainty in this analysis comes from the low-energy sputter-yield values used to determine the screen grid erosion rates. Since there is no sputter-yield data in the literature over the voltage range of interest (24 V to 60 V), an extrapolation of sputter-yield data obtained at higher energies to the energy range of interest was performed using an approach described by Rawlin [44]. Since extrapolations are inherently uncertain, an uncertainty of ±50% was added to the calculated sputter-yield values. There are activities currently underway to measure the sputter-yield of molybdenum at low energy, but these have not yet produced reliable data [45]. In the meantime the analysis of the screen grid erosion captures this lack of knowledge in the form of increased failure risk. Finally, it should be noted, that the screeen grid, after the 8,000-hr test, showed very little erosion [42].

Table 2 Parameters for Eq. (1)

Symbol	Definition	Values
A_b	Active grid area [m2]	0.06587
e	Electron charge [coul.]	1.6×10^{-19}
f_b	Beam current flatness parameter	0.40 to 0.46
f_d	Double ion ratio correction to centerline parameter	1.40 to 1.67
J_b	Beam Curent [A]	1.76 ± 1%
m_g	Mass of screen grid atom [kg]	1.59×10^{-25}
R_+^{++}	Measured double to single ion current ratio	0.15 to 0.20
t_s	Screen grid thickness [m]	3.80×10^{-4}
V_d	Discharge voltage [V]	24.5 to 26.0
Y_+	Single ion sputter yield = $1.06\times10^{-5} + (V_d\text{-}24.8)^2$ [atoms/ion]	±50%
Y_{++}	Double ion sputter yield = $1.06\times10^{-5} + (2V_d\text{-}24.8)^2$ [atoms/ion]	±50%
ρ	Density of screen grid material [kg/m3]	10220
ϕ_i	Screen grid transparency to ions	0.82
ϕ_s	Screen grid open area fraction	0.67

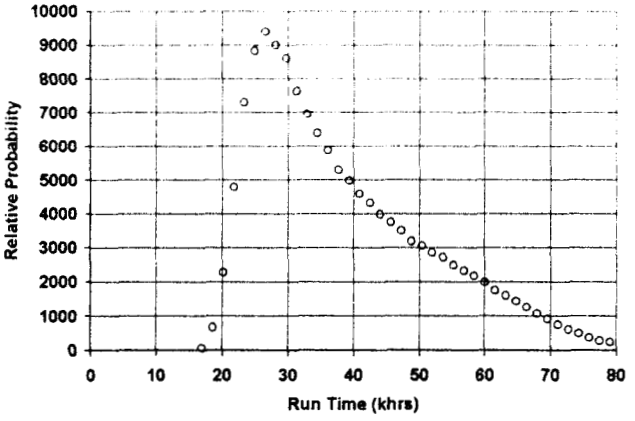

Fig. 5 Failure probability distribution for screen grid wear-out.

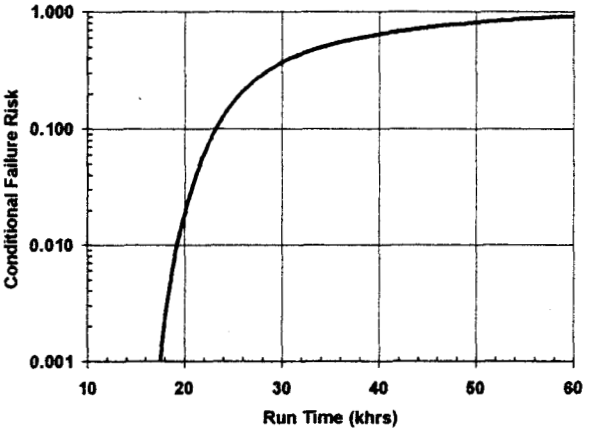

Fig. 6 Screen grid failure risk versus run time at full power.

Cathode Keeper Failure. The NSTAR thruster employs an enclosed cathode keeper assembly. This keeper assembly was added to reduce the amount of sputter-erosion on the cathode. The keeper electrode acts as a physical shield protecting the cathode, and as a result, the keeper itself is subject to ion sputtering. In the 8,000-hr test the keeper electrode lost 35% to 38% of its original thickness at a radial location approximately one third of the way between the edge of the keeper orifice and the outer diameter of the keeper [42]. A detailed analysis of this failure mode has not been performed, however, if this erosion rate is extrapolated linearly in time it suggests that the keeper will be eroded completely through after 21,000 to 23,000 hours of operation at full power. If greater margins are required, the keeper electrode could easily be made thicker in the region subject to the greatest erosion, or it could be made from a more sputter-resistant material [42].

Rogue Accelerator Grid Holes. Some of the material sputtered from the walls of the accelerator grid apertures gets deposited on the downstream surface of the screen grid. In the 8,000-hr test coatings on the screen grid as thick as 10 μm were measured [42]. These coatings could flake off and potentially short the grids. Sufficiently thick flakes will be unclearable by the grid clearing circuit. Prior to this, however, it is more likely that the sputter-deposited coatings will start to fail mechanically resulting in flakes of material that are loosely attached to the screen grid, but may now be intruding into the screen grid apertures. These intrusions will have the effect of defocusing the ion beamlets resulting in direct ion impingement on the accelerator grid. Direct ion impingement will cause rapid local erosion of the accelerator grid resulting in a significantly larger and asymmetric accelerator grid hole. Appearance of such "rogue" holes is not uncommon. One such hole was observed in the 1,000-hr test [37].

Any flake of material that comes to rest on the screen grid can also potentially cause the formation of rogue holes in the accelerator grid. During propulsion system operation there is a week force that will accelerate any loose material in the discharge chamber toward the screen grid. This differs from the ground test configuration used in the NSTAR life tests. In this configuration the engine is mounted horizontally so that the ion beam is approximately parallel to the Earth's surface. With this orientation, any loose material in the discharge chamber will not fall toward the grids, but rather will fall toward the side of the thruster. A few flakes of material were found at this location after the 8,000-hr test. In space, these flakes of material may have reached the screen grid and may have created rogue holes in the accelerator grid.

A rogue hole in the accelerator grid will be a problem only if it is sufficiently large that electon-backstreaming can occur or if the erosion geometry is such that it results in a piece of accelerator grid webbing coming loose and shorting the grids together. This places a premium on minimizing debris that can get into the engine and on keeping sputter-deposited material inside the engine from forming loose flakes.

Cathode Keeper Deposits. The NSTAR 8,000-hr test identified a new failure mode. This failure mode results from the deposition of material sputtered from the cathode orifice plate onto the upstream side of the cathode keeper electrode. Material deposits of up to

50 μm were found the conclusion of the 8,000-hr test [42]. These were by far the thickest material deposits found anywhere in the thruster. If this material flakes off, it could short the keeper to the cathode, making ignition of the cathode much less likely, or it could short the accelerator system electrodes with a material flake that may be too big to be cleared with the grid clearing circuit. At this time the maximum size of a molybdenum or tungsten flake that can be cleared by the grid clearing circuit is unknown, but there are plans for the NSTAR program to obtain this information. In addition, slight modifications to the keeper could be made to significantly improve the adherence of sputter-deposited material. For the thruster used in the 8,000-hr test this surface was not subjected to any kind of flake containment treatment since it was not recognized as a significant deposition site prior to the 8,000-hr test.

Hollow Cathode Life. The end of life for a hollow cathode will typically manifest itself as a failure to start. This will occur when there is insufficient low-work function material available at the emitter surface to provide enough free electrons at the cathode's ignition temperature to initiate breakdown of the xenon gas for the applied ignition voltage. Higher temperatures and higher ignition voltages facilitate cathode ignition. The cathode is engineered to establish an insert temperature typically between 1100°C and 1200°C for startup. The ignition voltage is limited to 650 V for the NSTAR engine because this voltage level has been shown to produce reliable cathode ignition in the Space Station Plasma Contactor development program. Higher voltages are possible, but come at the expense of increased complexity associated with handling the higher voltage level.

The longest duration test of a xenon hollow cathode on record is the 28,700-hr test performed by Sarver-Verhey [46, 47]. This cathode is the same diameter and uses the same insert as the NSTAR ion engine cathode, and was operated at an emission current of 12 A for the entire endurance test. The test was terminated when the cathode failed to start after 28,700 hours. Post-test analysis of the cathode confirmed that the cathode insert had reached the end of its service life [47]. This test demonstrated a total emitted charge capability of 334,000 A-hrs. Inspection of the test results, however, indicates that after 23,000 hours the cathode temperature started to rise rapidly [47]. In addition, the voltage required to ignite the cathode exceeded the 650-V capability of the NSTAR ignitor circuit at this time. Therefore, a more conservative estimate would place the cathode end-of-life at 23,000 hours for a total charge transfer of 276,000 A-hrs.

The emission current for the NSTAR ion engine at full power changes as a function of time as the accelerator grid apertures enlarge due to ion sputtering. For the first 2,000 hours of the 8,000-hr test the discharge current was between 13 A and 14 A. Between 2,000 hrs and 4,000 hrs the discharge current increased to 15 A and the discharge current stayed roughly between 15.0 A and 15.5 A over the last 4,000 hours of the test [42]. In the ongoing ELT the discharge current at full power has increased slowly from about 14 A at 500 hours to 14.5 A at 4,300 hours [33]. The discharge current in the ELT is slightly lower than that in the 8,000-hr test because the discharge voltage is slightly higher. The higher discharge voltage is believed to be the result of the ELT flow rates being approximately 2% lower than in the 8,000-hr test. The higher discharge voltage will affect the screen grid life so there is a trade-off between screen grid life and cathode life.

The cathode emission current is the difference between the discharge current and the beam current. Assuming a constant discharge current of 15 A and a beam current of 1.76 A, the emission current is 13.2 A. If the total emitted charge capability of the cathode is given by the lower estimate of 276,000 A-hrs, then the cathode life is 20,800 hours for thruster operation at full power. If the higher value for total emitted charge capability is used, i.e., 334,000 A-hrs, then the cathode life is 25,000 hours. These estimates, unfortunately, are highly uncertain since the rate at which the low-work-function material gets depleted in the cathode is known to be a function of the insert temperature, and how the temperature of the insert for the cathode inside the NSTAR ion engine relates to the insert temperature for the cathode in the 28,700-hr test is unknown. The cathode thermal environment in Sarver-Verhey's test is substantially different than that inside the ion engine. Probabilistic modeling of the cathode life has not been performed so this uncertainty cannot currently be quantified.

Grid shorts. The relatively small separation between the screen and accelerator grids (approximately 0.6 mm) can easily be bridged by debris from many sources resulting in a grid short. For this reason the NSTAR PPU includes a grid-clearing circuit whose sole function is to remove this debris and re-establish the ability of the accelerator system to stand-off the total voltage applied between the grids. The grid-clearing circuit and its capabilities are described in

detail by Goodfellow [48]. There are numerous debris sources that are not related to thruster wear, but rather are byproducts of the thruster, spacecraft and/or launch vehicle fabrication and cleanliness. These sources of debris, while important, do not contribute to wear-out failures. (One exception could be debris that comes to rest on the screen grid causing the formation of rogue holes in the accelerator grid.)

Wear-related debris comes from the flaking or spalling of sputter-deposited material. There are three principle locations that could be sources for this material. The first is the walls of the discharge chamber. The discharge chamber walls receive a net deposition of material sputtered primarily from the screen and accelerator grids. In the 8,000-hr test the thickest films found on the discharge chamber walls were only about 10 μm thick [42]. The walls of the discharge chamber are covered with a grid-blasted wire mesh designed to inhibit the spalling of sputter-deposited material. The limitations of this sputter-containment approach are not known, but its likely that coatings several times that observed in the 8,000-hr test can be successfully prevented from spalling. Consequently, flaking of material sputter-deposited on the walls of the discharge chamber is not believed to be a significant failure risk for the ST4 mission.

The second source location for material flakes is the downstream side of the screen grid. As mentioned earlier, this location receives a net deposition of material sputtered from the accelerator grid. Flakes formed in this region are very likely to short the grids if they are physically large enough to bridge the gap. If this occurs, continued operation of the engine must rely on the successful removal of this short by the grid-clearing circuit.

The third source location for material flakes, was also mentioned earlier, and that was the upstream side of the keeper electrode. Sputter-deposits of tungsten films as thick as 50 μm were found at this location after the 8,000-hr test. Thick, tungsten flakes may be difficult for the grid-clearing circuit to clear, therefore, preventing these coatings from flaking off should be a high priority for the ST4 ion engine design.

Accelerator Grid Structural Failure. Structural failure of the accelerator grid due to erosion by charge-exchange ions has been studied extensively [34,35,37,38,40,41]. These studies calculate the time to structural failure of the accelerator grid based on the removal of material from the "pits & grooves" erosion pattern that characterizes the wear on the downstream surface of the accelerator grid. End of life is defined when the erosion pattern penetrates completely through the grid thickness at the center of the grid. The time required to do this is given by,

$$T_{ag} = \frac{A_b(1-\phi_a)\alpha f_a e \rho t_a}{J_b \alpha_a \beta Y \lambda_{pg} m_g} \qquad (2)$$

Table 3 Parameters for Eqs. (2)

Symbol	Definition	Values
A_b	Active grid area [m2]	0.06587
e	Electron charge [coul.]	$1.6\text{x}10^{-19}$
f_a	Accelerator grid mass loss flatness parameter	0.41 to 0.61
J_b	Beam Curent [A]	$1.76 \pm 1\%$
m_g	Mass of screen grid atom [kg]	$1.59\text{x}10^{-25}$
V_a	Accelerator grid voltage [V]	180 to 250
V_{bp}	Ion beam plasma potential [V]	4 to 10
V_g	Neutralizer coupling voltage [V]	11 to 15
V_i	Ion energy for sputter-yield calculation [V]	$= V_a + V_g + V_{bp}$
t_a	Accelerator grid thickness [m]	$5.08\text{x}10^{-4}$
Y	Sputter yield at mormal incidence [atoms/ion]	$= -0.1935 + 2.622\text{x}10^{-3}V_i - 9.97\text{x}10^{-7}V_i^2$
α	Eroded area fraction	$= 0.12525 + (0.53973 w_g \text{x}10^3)$
α_a	Accelerator grid current to beam current ratio	0.35
β	Fraction of accelerator grid current striking the pits & grooves erosion pattern	0.7 to 0.8
λ_{pg}	Sputter yield parameter for pits & grooves erosion	$0.081/\beta$ to $0.286/\beta$
ϕ_a	Accelerator grid open area fraction	0.24
w_g	Width of the pits & grooves erosion pattern at the center of the grids [m]	$4.50\text{x}10^{-4}$ to $5.75\text{x}10^{-4}$

where the parameters and their values or ranges of values are defined in Table 3. The ranges given in this table represent the best current understanding of the possible values that each of these parameters can have. The parameters α and f_a, characterize the uncertainty in the erosion geometry. The spread in values given for these parameters is consistent with the variability observed in the NSTAR long-duration test program. The parameters β and λ_{pg} capture the uncertainty in the erosion rate in the pits and grooves pattern. For a given value of β, the value of λ_{pg} is selected from a range that depends on β so that the resulting erosion rates are also within the variability observed in the NSTAR long-duration tests. The intrinsic variability of these parameter is expected to be smaller than that represented in Table 3 so that these ranges will likely be reduced as more information is obtained.

Using Eq. (2) in the same probabilistic methodology described for the screen grid erosion characterized by Eq. (1) results in a B1 life (1 chance in 100 of failing) of about 22,000 hours for a fixed accelerator grid voltage of -180 V. If instead, the accelerator grid voltage is fixed at -250 V (the limit of the accelerator supply in the NSTAR PPU), then the B1 life is reduced to about 15,000 hours as indicated in Fig. 7.

Electron-backstreaming. Electron-backstreaming occurs when the accelerator grid can no longer prevent electrons in the beam plasma from traveling back into the positive-high-voltage engine. The magnitude of the negative voltage applied to the accelerator grid that is required to prevent electron-backstreaming is primarily a function of the positive high voltage, the thickness of the accelerator grid, the screen-accelerator grid separation, the ion current density, and the accelerator grid hole diameter.

Computer models can readily calculate the effects of these parameters on the local potential across the accelerator grid aperture. An axisymmetric code, written by K. Ishihara and Y. Arakawa of the University of Tokyo, provides a very simple tool to illustrate these effects. When using this code in this study, the onset of electron-backstreaming was defined, for a given geometry, as the smallest magnitude accelerator grid voltage which would result in no negative equipotential contours spanning the accelerator grid aperture. With no negative voltage coutours spanning the grid aperture, there is no potential barrier to prevent the backstreaming of electons. While this definition is probably not strictly correct, it is expected to be a reasonable approximation because the temperature of the electrons in the beam plasma is low (typically 1 or 2 eV).

Erosion of the accelerator grid apertures by ion sputtering during normal engine operation will increase the hole diameters as a function of run time. The effect of accelerator hole diameter increase on the electron-backstreaming voltage is given in Fig. 8 based on the Ishihara-Arakawa code. The calculations were made for an ion current density corresponding to a normalized perveance per hole of 2.1×10^{-9} A/V$^{3/2}$, a beam voltage of 1100 V, a discharge voltage of 25 V, and a discharge chamber electron temperature of 5 eV. The normalized perveance per hole (NPPH) is proportional to the ion current density and is defined in

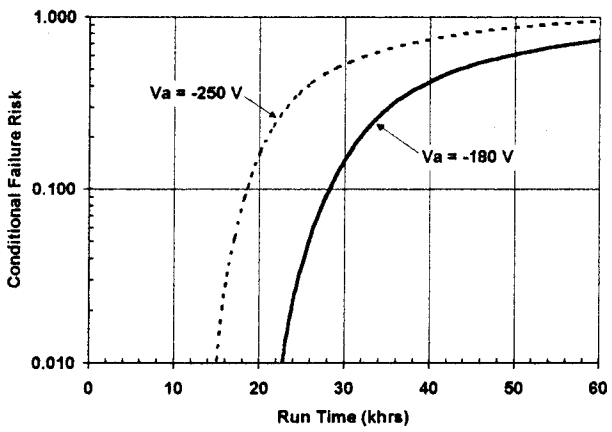

Fig. 7 Risks for accelerator grid structural failure with –180 V and –250 V on the accelerator grid.

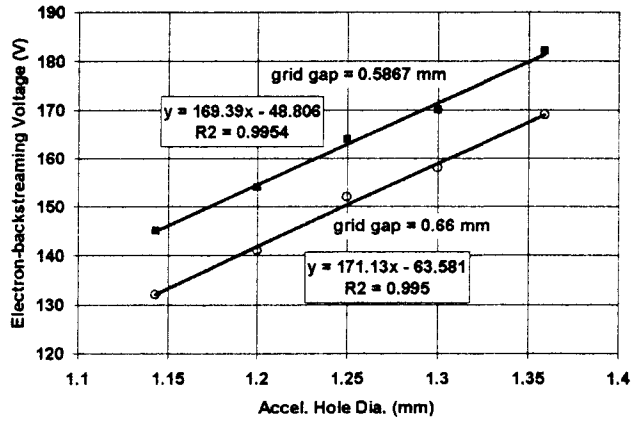

Fig. 8 The electron-backstreaming voltage is a linear function of the accelerator grid hole diameter.

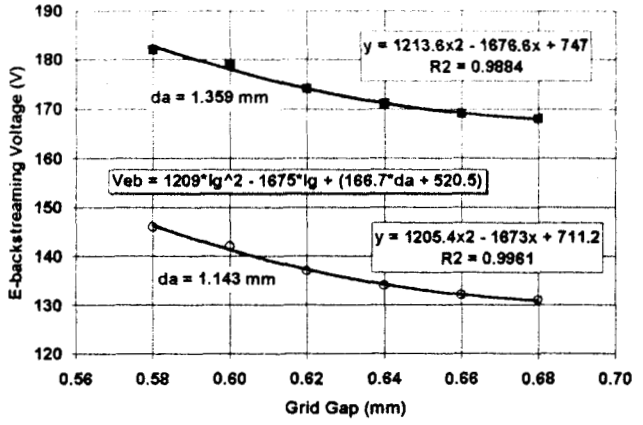

Fig. 9 The electron-backstreaming voltage is very sensitive to the grid gap.

Ref. 49. The value of 2.1×10^{-9} A/V$^{3/2}$ corresponds to the value expected at the center of the NSTAR grids for operation at full power. Changes in the discharge voltage and discharge chamber electron temperature have only very minor effects on the electron-backstreaming voltage and can be safely neglected.

The electron-backstreaming voltage is seen to be a linear function of the accelerator grid hole diameter with a slope of about 170 V/mm. In addition, the electron-backstreaming voltage is a non-linear function of the grid gap as shown in Fig. 9. The slopes of the curves in Fig. 9 range from about 80 to 250 V/mm for the given span of grid gaps. Consequently, a 0.01-mm change in the grid separation could change the electron-backstreaming voltage by a couple of volts. The data in Figs. 8 and 9 can be combined to provide the following expression for the electron-backstreaming voltage as a function of the grid gap, l_g, and the accelerator hole diameter, d_a, for the NPPH and beam voltage given above,

$$V_{eb} = 1209 l_g^2 - 1675 l_g + 166.7 d_a + 520.5 \quad (3)$$

where V_{eb} is in volts for l_g and d_a in milimeters.

Enlargement of the accelerator grid apertures is caused by ion sputtering. It should, therefore, be a straightforward process to calculate the rate at which the aperture diameter increases for operation at full power. Unfortunately, the fabrication of the grid apertures uses a 50/50 chemical etching process. This results in a hole that does not have straight cylindrical walls, but rather has a cusp-like geometry when viewed in cross-section [42]. Thus, even for constant operating conditions, the accelerator apertures may initially enlarge rapidly as the cusps are removed and then subsequently increase at a slower rate.

To simplify the problem, the cross-section of the cusps were approximated as triangles as shown in Fig. 10. With this simplifying geometry and the assumption that all of the ion flux responsible for eroding the accelerator grid apertures first removes the cusps before eroding any other part of the hole wall, the rate of increase of the accelerator grid holes can be calculated. Once the cusp is removed the diameter of the accelerator grid aperture as a function of run time may be given as,

$$d_a = \left[\frac{4 J_b \alpha_a Y m_g T (1-\beta) \lambda_h}{\pi \rho e t_a f_a N_h} + d_0 \right]^{1/2} \quad (4)$$

were d_0 is the accelerator grid hole diameter after the cusp has been removed. The rest of the parameters in this equation are defined in Tables 3 and 4.

The value for the combination of parameters, $(1-\beta)\lambda_h / f_a$ cannot be specified a priori. Consequently, the value for $(1-\beta)\lambda_h / f_a$ was selected so that the final accelerator grid hole diameter calculated from Eq. (4) with T = 8.2 khrs, and accounting for the time required to remove the cusps, would agree with the post-8,000-hr-test measurements of the hole diameter in the center of the grid [42]. To force this agreement requires that,

$$\frac{(1-\beta)\lambda_h}{f_a} = 0.371 \quad (5)$$

which is not unreasonable.

Combining Eqs. 3, 4 and 5 and accounting for the erosion of the cusps enables calculation of the electron-

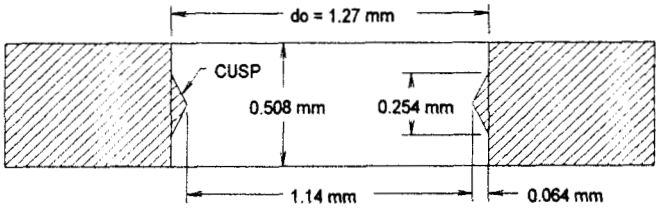

Fig. 10 Model of accelerator grid aperture and cusp geometry.

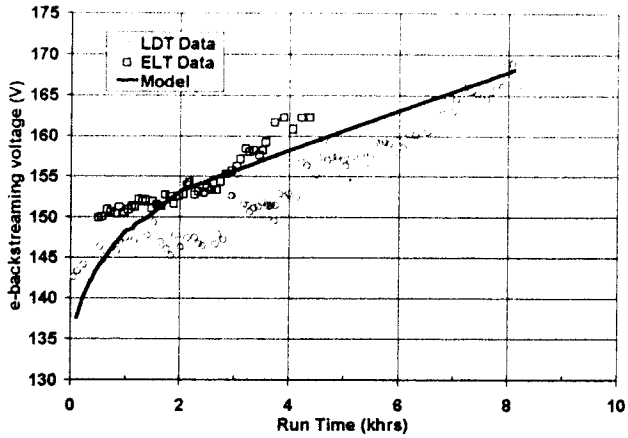

Fig. 11 Comparison of the electron-backstreaming model with data from the 8,000-hr LDT and the ongoing ELT.

backstreaming voltage as a function of time for conditions corresponding to the 8,000-hr and ELT tests. Comparison of the model with the electron-backstreaming data from these tests [33,42] is given in Fig. 11 for a grid gap of 0.66 mm. The data in this figure indicates that the model slightly under predicts the slope of the electron-backstreaming variation with time. Thus, the model is optimistic when extrapolated to longer times. In addition, it shows that the transient associated with the removal of the cusps lasts approximately 2,000 hours.

The model can be recast to calculate the time required to reach the onset of electron-backstreaming. This time is given as,

$$T_{eb} = \left(D^2 - d_0^2\right)\left(\frac{\pi\rho\, t_a e f_a N_h}{4 J_b \alpha_a Y m_g (1-\beta)\lambda_h}\right) \qquad (6)$$

where,

$$D = \frac{V_a - 1209 l_g^2 + 1675 l_g - 520.5}{166.7} \qquad (7)$$

represents the hole diameter at which electron-backstreaming occurs for an accelerator voltage of V_a. The actual time to the onset of electron-backstreaming is given by Eq. (6) plus the time required to remove the cusps (approximately 2,000 hours). The values or ranges of values for the parameters in Eqs. 6 and 7 are given in Tables 3 and 4. In these equations, the

Table 4 Parameters for Eqs. (3)-(7)

Symbol	Definition	Values
d_0	Accelerator grid hole diameter after the cusp has been removed [m]	$1.27\text{x}10^{-3}$
l_g	Screen-Accelerator grid gap [m]	$5.9\text{x}10^{-4}$ to $6.6\text{x}10^{-4}$
N_h	Number of holes in the accelerator grid	15,400
T	Run Time [s]	
λ_h	Sputter yield parameter for hole erosion	0.5 to 1.0
ρ	Density of accelerator grid material [kg/m^3]	10220

parameters f_a and l_g affect the erosion geometry, while the parameters β and λ_h affect the erosion rate. The allowable ranges of values for f_a, β and λ_h result in possible values for $(1-\beta)\lambda_h/f_a$ that can be approximately a factor of two greater than or less than that given in Eq. (5). In addition, the allowable values of β and λ_h permit a factor of three variation in the erosion rate of the accelerator grid holes.

With these values a Monte Carlo simulation, assuming a constant accelerator grid voltage of -180 V, results in the failure risk shown as the left-most curve in Fig. 12. This curve shows that there is a very high probability that electron-backstreaming will occur before 16,000 hours of operation at full power. Indeed, there is a 50% chance that it will occur at 10,000 hours. The calculated distribution of total mass loss rates from the holes is given in Fig. 13. The mass loss rate from the holes in the 8,000-hr test was estimated to be approximately 1.1 g/khr [42]. The higher erosion rates calculated in the simulation result from the lack of knowledge regarding the allowable values of some of the key parameters. As before, this lack of knowledge shows up as an increased failure risk.

To delay the onset of electron backstreaming, the magnitude of the accelerator voltage could be increased. The NSTAR PPU has the capability to operate with an accelerator grid voltage as negative as -250 V. Rerunning the Monte Carlo simulation with the accelerator grid voltage fixed at this level results in the middle curve in Fig. 12. This change has increased the B1 life from about 5,000 hours to approximately 16,000 hours. Clearly, the beneficial effect of making the accelerator grid more negative outweighs the increased erosion rate associated with the greater

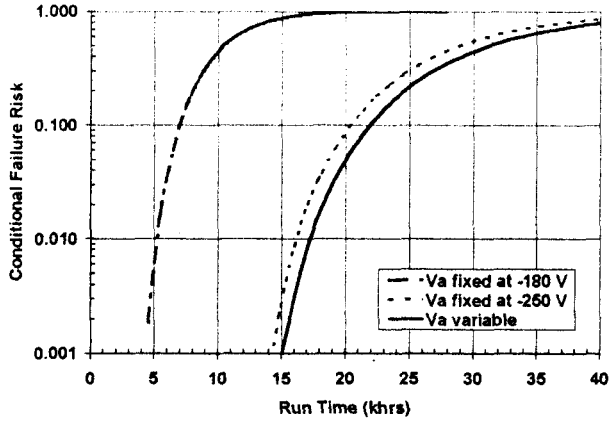

Fig. 12 Electron-backstreaming failure risk for fixed accelerator grid voltages of –180V and –250V and for the case where the accelerator grid voltage is decreased step-wise from –180V to –250 V.

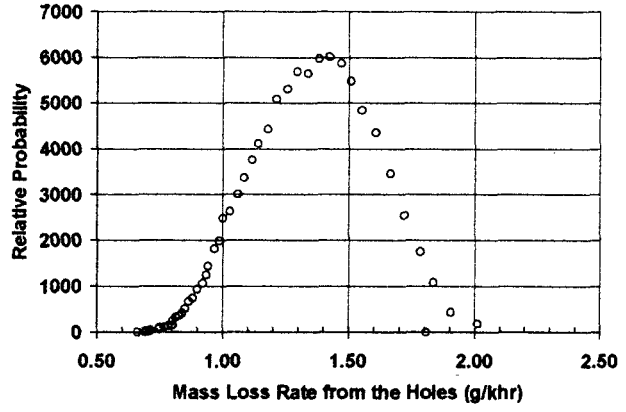

Fig. 13 Distribution of calculated total mass lost from the accelerator grid holes at failure.

voltage magnitude. However, the more negative accelerator grid also increases the erosion rate on the downstream surface of the grid as was shown in Fig. 8.

A further refinement can be obtained by increasing the magnitude of the accelerator grid voltage in discrete increments to maintain a specified voltage margin from the electron-backstreaming limit. The right-most curve in Fig. 12 shows the results of such a calculation where the accelerator grid voltage was made more negative in 10 V increments and a minimum 10 V margin was maintained from the electron-backstreaming limit until the -250 V limit of the accelerator grid power supply was reached. This approach appears to have only a minor benefit for this failure mode.

Combined Failure Modes

The data in Fig. 12 demonstrate that accelerator grid voltages more negative than -180 V will be required to prevent electron-backstreaming for engine lifetimes of the order of that required by the ST4 mission. Making the accelerator grid more negative will increase the erosion rate in the pits & grooves pattern on the downstream side of the grid and hasten the structural failure of the grid. Thus, these two failure modes are coupled.

These failure modes are further coupled by the grid geometry. With an accelerator grid voltage of -250 V the accelerator grid holes can erode to a diameter which will intersect the pits & grooves erosion pattern before they are large enough to reach the onset of electron-backstreaming. Thus, the maximum allowable accelerator grid hole diameter is not dictated by the limit of the accelerator grid power supply, but rather by the width of the pits & grooves erosion pattern. For the 8,000-hr test this width ranged from about 450 to 575 μm at the center of the grid and was found to be approximately constant in time during the 8,000-hr test [42]. The center-to-center hole spacing for the NSTAR grids is 2.2098 mm. Therefore, the maximum diameter the accelerator holes can grow to before intersecting the pits & grooves erosion pattern is

$$1.63 \text{ mm} < (d_a)_{max} < 1.76 \text{ mm} \qquad (8)$$

A Monte Carlo simulation of the coupled failure modes using the parameter values in Tables 3 and 4 results in the failure risk curve given in Fig. 14. This curve indicates that the B1 life for the accelerator grid is about 16,000 hours. In addition, this simulation indicated that about 24% of the failures are due to erosion in the pits & groove pattern, and 76% of the failures are due to accelerator grid aperture enlargement. The failure distribution for this case is given in Fig. 15. The peak of the failure distribution occurs at approximately 26,000 hours.

The accelerator grid failure risk is compared to that for the screen grid in Fig. 16. The left-hand tail of both of the failure distributions is driven by uncertainty in the behavior of critical parameters in the model. Never-the-less, even with this added risk due to shortcomings in our understanding, the calculated failure risks for the required 16,000-hr service life are less than 1 in 100, which is acceptable. In addition, it should again be remembered that these calculations are

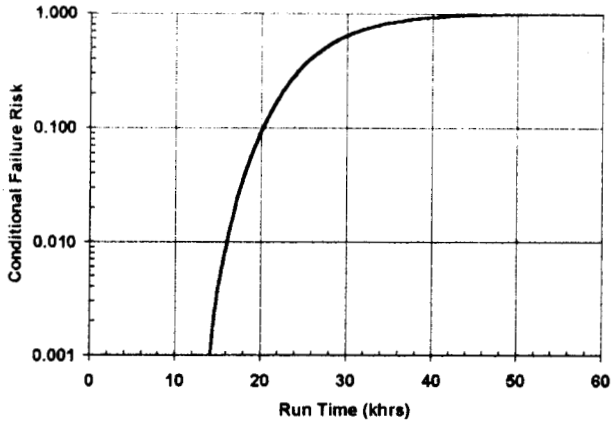

Fig. 14 Accelerator grid failure risk for the combined failure modes of electron-backstreaming and structural failure due to erosion on the downstream surface of the grid.

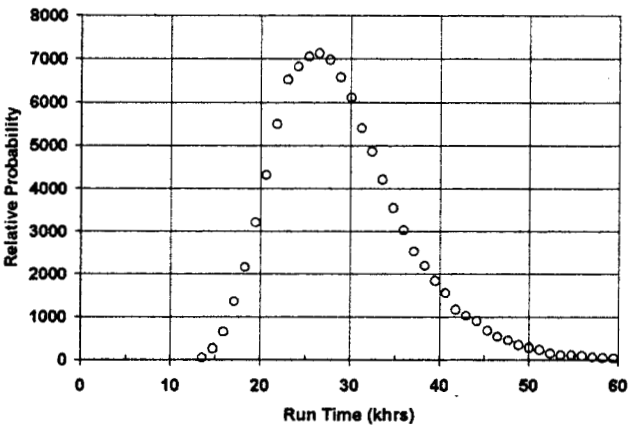

Fig. 15 Accelerator grid failure distribution for the combined failure modes.

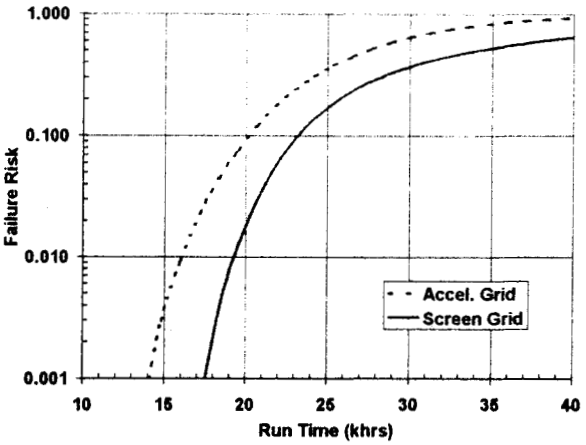

Fig. 16 Comparison of screen grid and accelerator grid failure risks.

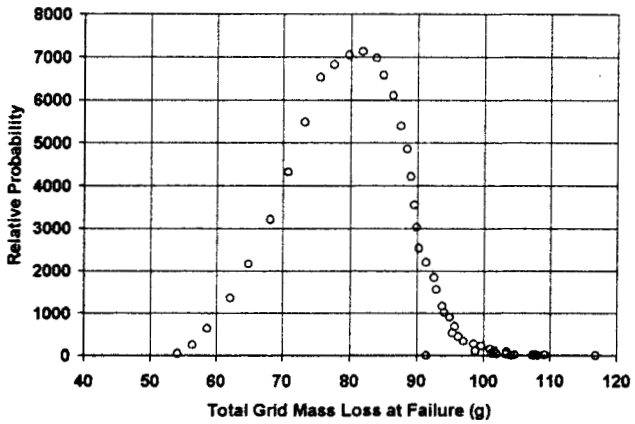

Fig. 17 Calculated distribution of total mass lost from the accelerator grid at failure for the combined failure modes.

for operation at full power which is the most stressing case. Therefore, even though the lower slope exhibited by the model in Fig. 11 may make the electron-backstreaming model slightly optimistic the conservatism implied by considering only full power operation is believed to result in the overall model still being conservative

Finally, the total calculated mass loss from the accelerator grid at failure (either structurally or from electron-backstreaming) is given in Fig. 17. The most probable value corresponds to a mass loss of approximately 80 g.

Conclusions

Ion propulsion is an enabling technology for the ST4/Champollion comet lander mission in the sense that it makes the mission affordable. The ST4 ion propulsion system is a three-engine version of the NSTAR hardware that is currently flying on DS1. This system will carry 385 kg of xenon to provide a ΔV of 11.4 km/s. Mass and cost constraints place a high premium on being able to accomplish this mission with only three NSTAR ion engines. This requires that the engines be capable of processing approximately 160 kg

of xenon each, or nearly twice the original propellant throughtput objective for the NSTAR program.

A detailed review of the history of ion engine endurance testing and the endurance test experience obtained through the NSTAR program has resulted in the identification of ten potentially significant wear-out failure modes. These failure modes include: electron-backstreaming due to enlargement of the accelerator grid apertures; structural failure of the accelerator grid; unclearable grid shorts; depletion of the cathode low-work-function material; accelerator grid failure due to rogue-hole formation; structural failure of the keeper orifice plate; structural failure of the screen grid; failure of the neutralizer due to plume-mode operation; and failure of the cathode or neutralizer heater from thermal cycling. Probabilistic modeling of the screen and accelerator grid failure modes indicates that these modes do not pose an unacceptable risk for the ST4 mission. Less sophisticated evaluation of the other failure modes also suggests that none of these pose unacceptable risks. Therefore, performing the ST4 mission the three-ion-engine system currently baselined appears to be within the capability of the NSTAR ion engine.

Acknowledgments

The work described in this paper was conducted at the Jet Propulsion Laboratory under a contract with the National Aeronautics and Space Administration.

References

1. http://nmp.jpl.nasa.gov/st4/
2. Park, R. A., et al., "Solar-Electric Propulsion Missions to the Comets," Paper presented at the AAS Meeting, Boston, MA, May 26, 1967.
3. Michielsen, H. F., "A Rendezvous with Halley's Comet in 1985-86," *J. Spacecraft and Rockets*, Vo. 5, No. 3, March 1968, pp. 328-334.
4. Kruse, D. H. and Fox, M. K., "Trajectory Analysis of Low Thrust and Ballistic Rendezvous Missions to Halley's Comet," Rept. ERR-FW-794, 1968, General Dynamics, Fort Worth, TX; also AIAA Paper No. 69-933, Princeton, NJ, 1969.
5. Kaufman, H. R. and Reader, P. D., "Experimental Performance of an Ion Rocket Employing an Electron-Bombardment Ion Source," Paper 1374, American Rocket Society, Inc., 1960.
6. Odom, P. R., Cikanek, H. A., and Allen, L. C., "Application of Solar Electric Propulsion to Comet and Asteroid Rendezvous and Docking (CARD) Missions with Sample Return," AIAA Paper No. 72-470, April 17-19, 1972.
7. Guttman, C. H. et al., "The Solar Electric Propulsion Stage Concept for High Energy Missions," AIAA Paper No. 72-465, April 17-19, 1972
8. Sauer, C. G., "Trajectory Analysis and Performance for SEP Comet Encke Missions," AIAA Paper No. 73-1059, Oct. 31-Nov. 2, 1973.
9. Ross, R. G., "Thruster Array Approaches for a Solar Electric Propulsion Encke Flyby Mission, AIAA Paper No. 73-1115, Oct. 31-Nov. 2, 1973.
10. Stuart, J. R., "System Design of an Ion Drive Spacecraft," AIAA Paper No. 78-643, presented at the AIAA/DGLR 13th International Electric Propulsion Conference, April 25-27, 1978.
11. Sauer, C. G., "SEPS Comet Rendezvous Perfromance Assessment," AIAA Paper No. 80-1685, August 11-13, 1980.
12. Yen, C. L., "Mission Options for the First SEPS Application,"AIAA Paper No. 81-186, presented at the AAS/AIAA Astrodynamics Specialist Conference, August 3-5, 1981.
13. Stuhlinger, E., Fechtig, H., Igenbergs, E., and Loeb, H., "Comet Nucleus Sample Return Missions with Electrically Propelled Spacecraft," J. of the British Interplanetary Society, Vol. 39, pp. 273-281, 1986.
14. Kerridge, S. J. and Atzei, A., "A Comet Nucleus Sample Return Mission," IAF-87-447, presented at the 38th Congress of the International Astronautical Federation, Oct. 10-17, 1987.
15. Sauer, C. G., "Application of Solar Electric Propulsion to Future Planetary Missions," AIAA-87-1053, presented at the 19th AIAA/DGLR/JSASS International Electric Propulsion Conference, May 11-13, 1987.
16. Sauer, C. G., "Current Trajectory Options for a Comet Nucleus Sample Return Mission," AAS 91-474, presented at the AAS/AIAA Astrodynamics Specialist Conference, Aug. 19-22, 1991.
17. Sauer, C. G., Planetary Mission Performance for Small Solar Electric Propulsion Spacecraft," AAS 93-561, presented at the AAS/AIAA Astrodynamics Specialist Conference, Aug. 16-19, 1993.
18. Kakuda, R., Sercel, J. and Lee, W., "Small Body Rendezvous Mission Using Solar Electric Propulsion: Low Cost Mission Approach and Technology Requirements," IAA-L-0710,

presented at the IAA International Conference on Low-Cost Planetary Missions, April 12-15, 1994.
19. Sauer, C. G. and Yen, C. L., "Planetary Mission Capability of Small Low Power Solar Electric Propulsion Systems," IAA-L-0706, presented at the IAA International Conference on Low-Cost Planetary Missions, April 12-15, 1994.
20. Sauer, C. G., "Solar Electric Performance for Medlite and Delta Class Planetary Missions," AAS 97-726, presented at the AAS/AIAA Astrodyanmics Specialist Conference, Aug. 4-7, 1997.
21. **http://www.estec.esa.nl/spdwww/rosetta/html/main.html**
22. Polk, J. E., et al., "In-Flight Validation of the NSTAR Ion Thruster Technology on the Deep Space One Mission," AIAA-99-2274, presented at the 35th AIAA/ASME/SAE/ASEE Joint Propulsion Conference, June 21-23, 1999.
23. Ganapathi, G. B. and Engelbrecht, C. S., "Post-Launch Performance Characterization of the Xenon Feed System on Deep Space One," AIAA99-2273, presented at the 35th AIAA/ASME/SAE/ASEE Joint Propulsion Conference, June 21-23, 1999.
24. Rawlin, V. K., et al., "NSTAR Flight Thruster Qualification Testing," AIAA-98-3936, presented at the 34th AIAA/ASME/SAE/ASEE Joint Propulsion Conference, July 6-9, 1998.
25. Sovey, J., et al., "Development of an Ion Thruster and Power Processor for New Millennium's Deep Space 1 Mission," AIAA-97-2778, Dec. 1997.
26. Pawlik, E. V., "An Experimental Evaluation of Array of Three Electron-Bombardment Ion Thrusters," NASA TN D-2597, January, 1965.
27. Pawlik, E. V. and Reader, P. D., "Accelerator Grid Durability Tests of Mercury Electron-Bombardment Ion Thrusters," NASA TN D-4054, July, 1967.
28. Masek, T. D., "Solar Electric Propulsion Thrust Subsystem Development," Technical Report 32-1579, Jet Propulsion Laboratory, California Institute of Technology, March 15, 1973.
29. Rawlin, V. K. and Mantenieks, M. A., "A Multiple Thruster Array for 30-cm Thrusters," AIAA Paper No. 75-402, March 19-21, 1975.
30. Fitzgerald, D. J., "Factors in the Design of Spacecraft Utilizing Multiple Electric Thrusters," AIAA Paper No. 75-404, March 19-21, 1975.
31. Lathem, W. C., "Particle and Field Measurements on Two J-Series 30-Centimeter Thrusters," NASA Technical Memorandum 81741, April, 1981.
32. Tierney, C. M., Brophy, J. R., and Mueller, J., "Plume Characteristics of a Multiple Ion Source Thruster," AIAA-95-3067, July 10-12, 1995.
33. Anderson, J. R., et al., "Results of an Ongoing Long Duration Ground Test of the DS1 Flight Spare Engine," AIAA-99-2875, presented at the 35th AIAA/ASME/SAE/ASEE Joint Propulsion Conference, June 21-23, 1999.
34. Polk, J. E., et al., "Probabilistic Analyses of Ion Engine Accelerator Grid Life," IEPC-93-176, presented at the 23rd International Electric Propulsion Conference, Seattle, WA, Sept. 1993.
35. Polk, J. E., Brophy, J. R., and Wang, J., "Spatial and Temporal Distribution of Ion Engine Accelerator Grid Erosion," AIAA-95-2924, presented at the 31st AIAA/ASME/SAE/ASEE Joint Propulsion Conference, July, 1995.
36. Patterson, M. J., et al., "2.3 kW Ion Thruster Wear Test," AIAA-95-2516, presented at the 31st AIAA/ASME/SAE/ASEE Joint Propulsion Conference, July, 1995.
37. Polk, J. E., et al., "A 1000-Hour Wear Test of the NASA NSTAR Ion Thruster," AIAA-96-2717, presented at the 32nd AIAA/ASME/SAE/ASEE Joint Propulsion Conference, July, 1996.
38. Brophy, J. R., Polk, J. E., and Rawlin, V. K., "Ion Engine Service Life Valication by Analysis and Testing," AIAA-96-2715, presented at the 32nd AIAA/ASME/SAE/ASEE Joint Propulsion Conference, July, 1996.
39. Polk, J. E., et al., "The Effect of Engine Wear on Performance in the NSTAR 8000 Hour Ion Engine Endurance Test," AIAA-97-3387, presented at the 33rd AIAA/ASME/SAE/ASEE Joint Propulsion Conference, July, 1996.
40. Polk, J. E., et al., "In Situ, Time-Resolved Accelerator Grid Erosion Measurements in the NSTAR 8000 Hour Ion Engine Wear Test," IEPC-97-047, presented at the 25th International Electric Propulsion Conference, Aug. 1997.
41. Anderson, J. R., Polk, J. E., and Brophy, J. R., "Service Life Assessment for Ion Engines," IEPC-97-049, presented at the 25th International Electric Propulsion Conference, Aug. 1997.
42. Polk., J. E., et al., "An 8200 Hour Wear Test on the NSTAR Ion Thruster," AIAA-99-2446, presented at the 35th AIAA/ASME/SAE/ASEE Joint Propulsion Conference, June 21-23, 1999.
43. Zakany, J. S. and Pinero, L. R., "Space Station Cathode Ignition Test Status at 32,000 Cycles,"

IEPC-97-167, presented at the 25th International Electric Propulsion Conference, Aug. 1997.
44. Rawlin, V. K., "Screen grid wear at low flow and high beam current conditions," NSTAR Memorandum, April 17, 1996, Glenn Research Center document.
45. Duchemin, O. and Polk, J. E., "Low Energy Sputtering Experiments for Ion Engine Lifetime Assessment, AIAA-99-2858, presented at the 35th AIAA/ASME/SAE/ASEE Joint Propulsion Conference, June 21-23, 1999.
46. Sarver-Verhey, T. R., "28,000 hour Xenon Hollow Cathode Life Test Results," IEPC-97-168, IEPC-97-167, presented at the 25th International Electric Propulsion Conference, Aug. 1997.
47. Sarver-Verhey, T. R., "Destructive Evaluation of a Xenon Hollow Cathode After a 28,000 Hour Life Test," AIAA-98-3482, presented at the 34th AIAA/ASME/SAE/ASEE Joint Propulsion Conference, July, 1998.
48. Goodfellow, K. D., "An Experimental and Theoretical Analysis of Grid-Short Clearing Capability of the NSTAR Ion Propulsion System," AIAA-99-2859, presented at the 35th AIAA/ASME/SAE/ASEE Joint Propulsion Conference, June 21-23, 1999.
49. Aston, G. and Kaufman, H. R., "The Ion-Optics of a Two-Grid Electron Bombardment Thruster," AIAA-76-1029, Nov. 14-17, 1976.